ZP4, an Improved Neuronal Zn²⁺ Sensor of the Zinpyr Family

Shawn C. Burdette,[†] Christopher J. Frederickson,[‡] Weiming Bu,[†] and
Stephen J. Lippard*,[†]

*Contribution from the Department of Chemistry, Massachusetts Institute of Technology,
Cambridge, Massachusetts, 02139, and NeuroBioTex, Incorporated, Galveston, Texas 77550*

Received September 28, 2002 ; E-mail: lippard@lippard.mit.edu

Abstract: A second-generation fluorescent sensor for Zn²⁺ from the Zinpyr family, ZP4, has been synthesized and characterized. ZP4 (Zinpyr-4, 9-(o-carboxyphenyl)-2-chloro-5-[2-{bis(2-pyridylmethyl)-aminomethyl}-N-methylaniline]-6-hydroxy-3-xanthanone) is prepared via a convergent synthetic strategy developed from previous studies with these compounds. ZP4, like its predecessors, has excitation and emission wavelengths in the visible range (~500 nm), a dissociation constant (K_d) for Zn²⁺ of less than 1 nM and a high quantum yields ($\Phi = \sim 0.4$), making it well suited for biological applications. A 5-fold fluorescent enhancement is observed under simulated physiological conditions corresponding to the binding of the Zn²⁺ cation to the sensor, which inhibits a photoinduced electron transfer (PET) quenching pathway. The metal-binding stereochemistry of ZP4 was evaluated through the synthesis and X-ray structural characterization of [M(BPAMP)(H₂O)$_n$]⁺ complexes, where BPAMP is [2-{bis(2-pyridylmethyl)aminomethyl}-N-methylaniline]-phenol and M = Mn²⁺, Zn²⁺ ($n = 1$) or Cu²⁺ ($n = 0$).

Introduction

Zinc is one of many transition metal elements that sustain life.[1] Once postulated to be readily available from a cytosolic pool of free metal ion,[2] mounting evidence suggests that Zn²⁺ uptake and distribution are regulated by a complex intracellular mechanism.[3–5] Disruption of Zn²⁺ homeostasis after ischemia,[6,7] seizures,[8–15] and following head injury[16] induces neuronal death. Although methods for detecting zinc show no evidence of perikaryal Zn²⁺ in healthy cells,[17,18] following these various traumas, damaged neuronal cells are stained intensely for this metal ion.[16,19–21]

In addition to acute toxicity, disruption of Zn²⁺ homeostasis may play a role in the pathology of several neurodegenerative disorders,[22,23] like the formation of amyloid plaques in Alzheimer's disease.[24–26] The highly regulated delivery of zinc to intracellular targets and the deleterious effects observed during overexposure to the free metal ion suggest that healthy cells contain no unbound Zn²⁺; however, free Zn²⁺ may play a vital role in communication between cells. Zinc released from glutamatergic nerve terminals plays a role in neurotransmission,[27–30] but the precise function of this synaptic Zn²⁺ remains unclear.[31–33] Extracellular Zn²⁺ has been implicated in the modulation of cellular processes through a zinc-sensing receptor.[34]

† Massachusetts Institute of Technology.

‡ NeuroBioTex, Inc.

(1) Vallee, B. L.; Falchuk, K. H. *Physiol. Rev.* **1993**, *73*, 79−118.
(2) Williams, R. J. P.; Fraústo da Silva, J. J. R. *Coord. Chem. Rev.* **2000**, *200−202*, 247−348.
(3) Outten, C. E.; O'Halloran, T. V. *Science* **2001**, *292*, 2488−2492.
(4) Hitomi, Y.; Outten, C. E.; O'Halloran, T. V. *J. Am. Chem Soc.* **2001**, *123*, 8614−8615.
(5) Outten, C. E.; Tobin, D. A.; Penner-Hahn, J. E.; O'Halloran, T. V. *Biochemistry* **2001**, *40*, 10 417−10 423.
(6) Koh, J. Y.; Suh, S. W.; Gwag, B. J.; He, Y. Y.; Hsu, C. Y.; Choi, D. W. *Science* **1996**, *272*, 1013−1016.
(7) Tonder, N.; Johansen, F. F.; Frederickson, C. J.; Zimmer, J.; Diemer, N. H. *Neurosci. Lett.* **1990**, *109*, 247−252.
(8) Choi, D. W.; Koh, J. Y. *Annu. Rev. Neurosci.* **1998**, *21*, 347−375.
(9) Canzoniero, L. M. T.; Turetsky, D. M.; Choi, D. W. *J. Neurosci.* **1999**, *19: RC31*, 1−6.
(10) Sheline, C. T.; Behrens, M. M.; Choi, D. W. *J. Neurosci.* **2000**, *20*, 3139−3146.
(11) Kim, A. H.; Sheline, C. T.; Tian, M.; Higashi, T.; McMahon, R. J.; Cousins, R. J.; Choi, D. W. *Brain Res.* **2000**, *886*, 99−107.
(12) Kim, Y.-H.; Kim, E. Y.; Gwag, B. J.; Sohn, S.; Koh, J.-Y. *Neuroscience* **1999**, *89*, 175−182.
(13) Noh, K.-M.; Koh, J.-Y. *J. Neurosci.* **2000**, *20: RC111*, 1−5.
(14) Park, J. A.; Lee, J.-Y.; Sato, T.-A.; Koh, J.-Y. *J. Neuroscience* **2000**, *20*, 9096−9103.
(15) Weiss, J. H.; Sensi, S. L.; Koh, J. Y. *TiPS* **2000**, *21*, 395−401.
(16) Suh, S. W.; Chen, J. W.; Motamedi, M.; Bell, B.; Listiak, K.; Pons, N. F.; Danscher, G.; Frederickson, C. J. *Brain Res.* **2000**, *852*, 268−273.
(17) Frederickson, C. J. *Int. Rev. Neurobiol.* **1989**, *31*, 145−238.
(18) Danscher, G. *Histochemistry* **1981**, *71*, 1−16.
(19) Sensi, S. L.; Canzoniero, L. M. T.; Yu, S. P.; Ying, H. S.; Koh, J. Y.; Kerchner, G. A.; Choi, D. W. *J. Neuroscience* **1997**, *17*, 9554−9564.
(20) Budde, T.; Minta, A.; White, J. A. *Neuroscience* **1997**, *79*, 347−358.
(21) Suh, S. W.; Danscher, G.; Jensen, M. S.; Thompson, R.; Motamedi, M.; Frederickson, C. J. *Brain Res.* **2000**, *879*, 7−12.
(22) Cuajungco, M. P.; Lees, G. J. *Neurobiol. Dis.* **1997**, *4*, 137−169.
(23) Bush, A. I. *Curr. Opin. Chem. Biol.* **2000**, *4*, 184−191.
(24) Suh, S. W.; Jensen, K. B.; Jensen, M. S.; Silva, D. S.; Kesslak, P. J.; Danscher, G.; Frederickson, C. J. *Brain Res.* **2000**, *852*, 274−278.
(25) Curtain, C. C.; Ali, F.; Volitakis, I.; Cherny, R. A.; Norton, R. S.; Beyreuther, K.; Barrow, C. J.; Masters, C. L.; Bush, A. I.; Barnham, K. J. *J. Biol. Chem.* **2001**, *276*, 20 466−20 473.
(26) Suzuki, K.; Miura, T.; Takeuchi, H. *Biochem. Biophys. Res. Comm.* **2001**, *285*, 991−996.
(27) Takeda, A. *Brain Res. Rev.* **2000**, *34*, 137−148.
(28) Thompson, R. B.; Whetsall, W. O., Jr.; Maliwal, B. P.; Fierke, C. A.; Frederickson, C. J. *J. Neurosci. Methods* **2000**, *96*, 35−45.
(29) Li, Y.; Hough, C. J.; Suh, S. W.; Sarvey, J. M.; Frederickson, C. J. *J. Neurophysiol.* **2001**, *86*, 2597−2604.
(30) Li, Y.; Hough, C. J.; Frederickson, C. J.; Sarvey, J. M. *J. Neurosci.* **2001**, *21*, 8015−8025.
(31) Cole, T. B.; Martyanova, A.; Palmiter, R. D. *Brain Res.* **2001**, *891*, 253−265.
(32) Lee, J.-Y.; Cole, T. B.; Palmiter, R. D.; Koh, J.-Y. *J. Neurosci.* **2000**, *20: RC79*, 1−5.
(33) Lee, J.-Y.; Park, J.; Kim, Y.-H.; Kim, D. H.; Kim, C. G.; Koh, J.-Y. *Exp. Neurol.* **2000**, *161*, 433−441.
(34) Herchfinkel, M.; Moran, A.; Grossman, N.; Sekler, I. *Proc. Natl. Acad. Sci. U.S.A.* **2001**, *98*, 11 749−11 754.
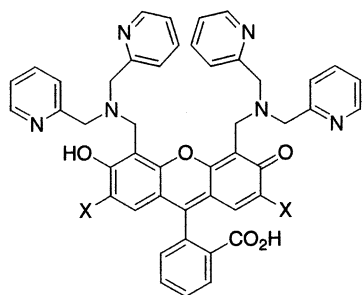
X = Cl : Zinpyr-1 : ZP1 : **1**
X = H : Zinpyr-2 : ZP2 : **2**

Figure 1. First members of the ZP family of fluorescein-based Zn²⁺ sensors ZP1 and ZP2. Both sensors incorporate a DPA ligand and have fluorescence properties amenable to biological studies.

Fluorescent sensors facilitate study of spectroscopically silent metal ions such as Zn^{2+} in biological systems[35-37] because specific properties can be engineered into probes through chemical synthesis. Moreover, fluorescence microscopy is both a sensitive and an innocuous investigative technique. To advance our studies of Zn^{2+} in neurobiology, we have designed and reported on a new family of Zn^{2+}-sensitive fluorescent probes (Figure 1).[38,39] ZP1 and ZP2 were the first in a series of fluorescein-based sensors designed to induce a positive fluorescence response upon complexation of Zn^{2+}. Although these two dyes offer several advantages over traditional Zn^{2+} sensors, improvements in the both the synthetic methodology and the physical properties of the sensor are desirable for an even more efficient investigation of Zn^{2+} ion in neurochemistry.

ZP1 can be prepared by a Mannich reaction in one step,[40] but the conditions limit the variety of metal-binding ligands that can be incorporated into the sensor. The preparation of ZP2 is more versatile,[38] but a low-yielding synthesis of the key intermediate reduces the rate at which compounds can be produced. In addition to these synthetic restrictions, both compounds have two distinct Zn^{2+} coordination sites. Although the binding affinities of the two sites for Zn^{2+} differ significantly, and only the first binding event is accompanied by a fluorescence change,[38] these properties may not apply to future sensors. Multiple metal ion binding events under physiological conditions complicate the analysis and can lead to ambiguous conclusions. One of the advantages of ZP sensors is the brightness of the Zn^{2+}-bound complex, yet the tertiary amines responsible for the fluorescence increase are susceptible to protonation at physiological pH. The inhibition of a photoinduced electron transfer (PET) pathway either by coordination to a closed-shell metal ion or protonation of an amine is a common strategy utilized in the design of intensity-based sensors.[41,42] Although the fluorescence intensity of the Zn^{2+}-bound complex is greater than that of the protonated sensor,

the magnitude of the fluorescence change upon metal binding is diminished and background fluorescence from the unmetalated probe is high at physiological pH.[39] In the second generation ZP sensor reported here, we have addressed these shortcomings with an improved synthetic strategy and a modified Zn^{2+}-binding ligand.

Experimental Section

Materials and Methods. Chlorobenzene and dichloroethane were distilled from CaH_2 under nitrogen. Acetonitrile was distilled from CaH_2 under nitrogen and dried over 3 Å molecular sieves, nitrobenzene and DMF were dried over 3 Å molecular sieves. THF was dried on an aluminum oxide column followed by a column of molecular sieves. $CDCl_3$ was dried over 3 Å molecular sieves. Di-(2-picolyl)amine (DPA) was prepared as previously described.[43] All other reagents were purchased and used as received. Flash column chromatography was performed with silica gel-60 (230−400 mesh), octadecyl-functionalized silica gel (RP18), or Brockman I activated basic aluminum oxide (150 mesh). Thin layer chromatographic (TLC) analysis was performed with Merck F254 silica gel-60, Merck RP-18 F254S, or Merck F254 aluminum oxide-60 plates and viewed by UV light, or developed with ceric ammonium molybdate, ninhydrin or iodine stain. NMR spectra were recorded on a Varian 500 MHz or 300 MHz spectrometer at ambient probe temperature, 283 K, and referenced to the internal ¹H and ¹³C solvent peaks. Infrared spectra were recorded on a BTS 135 or an Avatar 360 FTIR instrument as KBr pellets or thin films on NaCl plates. Electrospray ionization (ESI) mass spectrometry was performed in the MIT Department of Chemistry Instrumentation Facility (DCIF) with the use of *m*-nitrobenzyl alcohol as the matrix. **CAUTION: Several of the isolated compounds below contain perchlorate ion, which can detonate explosively and without warning. Although we have encountered no incidents with the reported compounds, all due precautions should be taken.**

2′-Carboxy-5-chloro-2,4-dihydroxybenzophenone (5). Phthalic anhydride (**3**, 9.0 g, 61 mmol) and 4-chlororesorcinol (**4**, 8.54 g, 59.1 mmol) were combined in $C_6H_5NO_2$ (150 mL) and chilled to 0 °C. Aluminum chloride ($AlCl_3$, 18.4 g, 138 mmol) was added slowly over 1 h, and the slurry was stirred overnight while warming to room temperature. The reaction mixture was heated to 120 °C for 6 h, and then diluted with 0.1 M HCl (700 mL) and hexanes (100 mL) to precipitate a black-brown solid. The solids were collected on a frit and dissolved in a boiling solution of methanol and water (1:1) and decolorizing carbon was added. The solution was filtered through Celite and the product crystallized at −10 °C. The solid was recrystallized twice (1:1 CH_3OH/water), washed with ice cold water and dried to give the product as a brown crystalline solid (8.45 g, 48.9%). TLC R_f = 0.26 (7:3 $CHCl_3$/MeOH). ¹H NMR (CD_3OD, 500 MHz) δ 6.47 (1 H, s), 6.94 (1 H, s), 7.38 (1 H, dd, J = 1.2, 7.2 Hz), 7.65 (1 H, td, J = 1.5, 7.5 Hz), 7.73 (1 H, td, J = 1.5, 7.2 Hz), 8.11 (1 H, dd, J = 1.5, 7.5 Hz). ¹³C NMR (CD_3OD, 125 MHz) 104.91, 113.32, 115.65, 128.64, 130.70, 131.14, 131.75, 133.78, 134.76, 141.54, 161.80, 164.78, 168.69, 202.41. FTIR (KBr) 3390, 2828, 2663, 2547, 1691, 1615, 1571, 1419, 1293, 1219, 1141, 925, 772. HRMS (ESI): Calcd for MH⁺ 293.0218; Found 293.0212.

2′-Chloro-5′-methylfluorescein Di-*t*-butyldimethylsilyl Ether (7). 2′-Carboxy-5-chloro-2,4-dihydroxybenzophenone (**5**, 5.00 g, 17.0 mmol) and 2-methylresorcinol (2.12 g, 17.0 mmol) were crushed and melted into a brown liquid at 150 °C. Fused $ZnCl_2$ (2.33 g, 110 mmol) was added slowly over 35 min, and the temperature was slowly increased to 250 °C over 30 min until the material solidified. The brick red solid was pulverized and boiled in 250 mL of 3 M HCl for 30 min. The red solid was collected on a frit, washed thoroughly with hot water and dried in vacuo. The crude product was filtered through a plug of silica

(35) Tsien, R. Y. *Chem. Eng. News* **1994**, *72*, 34−44.
(36) Kimura, E.; Koike, T. *Chem. Soc. Rev.* **1998**, *27*, 179−184.
(37) Lippard, S. C.; Lippard, S. J. *Coord. Chem. Rev.* **2001**, *216−217*, 333−361.
(38) Burdette, S. C.; Walkup, G. K.; Spingler, B.; Tsien, R. Y.; Lippard, S. J. *J. Am. Chem. Soc.* **2001**, *123*, 7831−7841.
(39) See Supporting Information in ref 38.
(40) Walkup, G. K.; Burdette, S. C.; Lippard, S. J.; Tsien, R. Y. *J. Am. Chem Soc.* **2000**, *122*, 5644−5645.
(41) Czarnik, A. W. *Acc. Chem. Res.* **1994**, *27*, 302−308.
(42) de Silva, A. P.; Gunaratne, H. Q.; Gunnlaugsson, T.; Huxley, A. J. M.; McCoy, C. P.; Rademacher, J. T.; Rice, T. E. *Chem. Rev.* **1997**, *97*, 1515−1566.

(43) Gruenwedel, D. W. *Inorg. Chem.* **1968**, *7*, 495−501.

(7:3 CHCl₃:MeOH) to give a red solid after solvent removal. The crude 2′-chloro-5′-methylfluorescein (**6**, mixture of two components with ~10% 4′,5′-dimethylfluorescein) was combined with imidazole (3.40 g, 101 mmol) in DMF (300 mL) and stirred. To the resulting red slurry was added *tert*-butyldimethylsilyl chloride (6.92 g, 45.9 mmol). The reaction mixture was stirred for 12 h at room temperature. A portion of the DMF was removed (~250 mL), and the reaction mixture was diluted with saturated brine (~300 mL). The aqueous layer was extracted with EtOAc, and the combined organic extracts were dried over MgSO₄ to give a brown oil after filtration and solvent removal. The crude product was filtered through silica (7:2:1 hexanes/C₆H₅CH₃/EtOAc) and the solvents removed. Flash chromatography (9:1 hexanes/EtOAc) yielded an impure brown solid (3.8 g) containing ~10% of the corresponding 4′,5′-dimethylfluorescein disilyl ether. A yield of 37% was calculated based on the integration of NMR peaks. TLC $R_f = 0.41$ (4:1 hexanes/EtOAc). ¹H NMR (CDCl₃, 500 MHz) δ 0.21 (6 H, s), 0.31 (6 H, s), 1.02 (9 H, s), 1.05 (9 H, s), 2.34 (3 H, s), 6.46−6.53 (2 H, m), 6.74 (1 H, s), 6.83 (1 H, s), 7.20 (1 H, d, $J = 7.5$ Hz), 7.64 (1 H, t, $J = 8.0$ Hz), 7.70 (1 H, t, $J = 7.0$ Hz), 8.03 (1 H, d, $J = 7.5$ Hz). ¹³C NMR (CDCl₃, 125 MHz) δ −4.17, −4.10, −4.03, −3.94, 9.58, 18.47, 18.54, 25.79, 25.85, 25.91, 83.43, 108.69, 111.62, 113.19, 116.70, 121.35, 124.21, 125.32, 125.43, 127.02, 128.95, 130.04, 135.28, 150.64, 151.07, 152.79, 153.37, 155.61, 169.42. FTIR (thin film) 2955, 2930, 2858, 1769, 1606, 1488, 1411, 1281, 1257, 1218, 1183, 1089. HRMS (ESI): Calcd for MH⁺ 609.2259; Found 609.2254.

2′-Chloro-5′-bromomethylfluorescein Di-*t*-butyldimethylsilyl Ether (8). 2′-Chloro-5′-methylfluorescein di-*tert*-butyldimethylsilyl ether (**7**, 3.80 g, 6.24 mmol, contains 10% 4′,5′-dimethylfluorescein disilyl ether), 1,3-dibromo-5,5-dimethylhydantoin (2.0 g, 7.0 mmol), and 1,1′-azobis-(cyclohexanecarbonitrile) (VAZO 88, 85 mg, 0.347 mmol) were combined in C₆H₅Cl (150 mL). Acetic acid (100 µL, 1.70 µmol) was added to the stirring solution, and the reaction mixture was stirred at 40 °C for 60 h. The crude reaction mixture was washed twice with hot water (100 mL, 80 °C), and the solvent was removed. Flash chromatography on silica (7:1 hexanes/EtOAc) yielded the product as a brown oil, (2.83 g, 73.3%). TLC $R_f = 0.28$ (7:1 hexanes/EtOAc). ¹H NMR (CDCl₃, 500 MHz) δ 0.28 (6 H, s), 0.30 (6 H, s), 1.04 (9 H, s), 1.05 (9 H, s), 4.83 (1 H, d, $J = 9.5$ Hz), 4.84 (1 H, d, $J = 9.5$ Hz), 6.56 (1 H, d, $J = 9.0$ Hz), 6.63 (1 H, d, $J = 9.0$ Hz), 6.92 (1 H, s), 7.22 (1 H, d, $J = 7.5$ Hz), 7.62 (1 H, td, $J = 1.0, 7.5$ Hz), 7.68 (1 H, td, $J = 1.0, 7.5$ Hz), 8.01 (1 H, dd, $J = 1.0, 7.5$ Hz). ¹³C NMR (CDCl₃, 125 MHz) δ −4.30, −4.24, −4.10, −4.01, 18.30, 22.00, 22.33, 24.37, 25.63, 25.76, 33.86, 82.38, 108.68, 111.98, 113.11, 114.57, 118.29, 121.72, 124.03, 125.20, 126.71, 128.68, 128.77, 130.13, 135.30, 150.36, 150.53, 152.12, 153.35, 155.83, 169.87. FTIR (thin film) 3208, 2954, 2931, 2858, 1730, 1608, 1582, 1453, 1429, 1282, 1257, 839. HRMS (ESI): Calcd for MH⁺ 687.1364; Found 687.1359.

2-[Bis(2-pyridylmethyl)aminomethyl]nitrobenzene (10). DPA (950 mg, 4.77 mmol), K₂CO₃ (6.50 g, 47.0 mmol), 2-nitrobenzylbromide (**9**, 980 mg, 4.54 mmol), and powdered 3 Å molecular sieves (750 mg) were combined in 20 mL of CH₃CN and stirred for 12 h under Ar. The crude reaction mixture was filtered through Celite to give a brown oil after solvent removal. Flash chromatography on basic alumina (7:3 CH₂Cl₂:EtOAc) yielded the product as an orange oil (997 mg, 65.7%). TLC $R_f = 0.26$ (7:3 CH₂Cl₂:EtOAc). ¹H NMR (CDCl₃, 500 MHz) δ 3.79 (4 H, s), 4.08 (2 H, s), 7.14 (2 H, td, $J = 1.0, 5.0$ Hz), 7.34 (1 H, td, $J = 1.0, 7.5$ Hz), 7.40 (2 H, d, $J = 7.5$ Hz), 7.49 (1H, dd, $J = 1.0, 7.5$ Hz), 7.64 (2 H, td, $J = 2.0, 7.5$ Hz), 7.71 (1 H, dd, $J = 0.5, 7.5$ Hz), 7.77 (1 H, dd, $J = 1.0, 8.0$ Hz), 8.51 (2 H, dq, $J = 1.0, 5.0$ Hz). ¹³C NMR (CDCl₃, 125 MHz) δ 56.06, 60.57, 122.33, 123.48, 124.52, 128.12, 131.57, 132.56, 134.55, 136.68, 149.10, 150.13, 158.77. FTIR (thin film) 3064, 3009, 2925, 2830, 1589, 1526, 1433, 1362, 766, 731. HRMS (ESI): Calcd for MH⁺, 335.1503; Found 335.1493.

2-[Bis(2-pyridylmethyl)aminomethyl]aniline (11). Pd/C (300 mg, 10% activated) and 2-[bis(2-pyridylmethyl)aminomethyl]-nitrobenzene (**10**, 2.48 g, 7.42 mmol) were combined in 150 mL of MeOH and stirred

under a hydrogen atmosphere (1 atm) for 24 h with the addition of 300 mg of Pd/C after 12 h. The reaction mixture was filtered through Celite to give a dark yellow oil after solvent removal. Flash chromatography on basic alumina with a solvent gradient (CHCl₃ to 9:1 CHCl₃/MeOH) yielded a yellow oil. Additional flash chromatography on basic alumina (99:1 CHCl₃/MeOH) yielded the product as a yellow oil (100 mg, 5%). TLC $R_f = 0.41$ (97:3 CHCl₃/MeOH). ¹H NMR (CDCl₃, 500 MHz) δ 3.65 (2 H, s), 3.79 (4 H, s), 4.94 (2 H, bs), 6.59−6.64 (2 H, m), 7.02−7.05 (2 H, m), 7.12 (2 H, td, $J = 1.0, 5.0$ Hz), 7.37 (2 H, d, $J = 7.5$ Hz), 7.59 (2 H, td, $J = 2.0, 7.5$ Hz), 8.53 (2H, dt, $J = 1.0, 5.0$ Hz). ¹³C NMR (CDCl₃, 125 MHz) δ 57.90, 60.22, 115.45, 117.23, 122.09, 122.33, 123.49, 128.55, 131.28, 136.43, 147.12, 149.18, 159.29. FTIR (thin film) 3396, 3320, 3209, 3009, 2921, 2805, 1615, 1590, 1494, 1433, 751. HRMS (ESI): Calcd for MH⁺ 305.1766; Found 305.1769.

9-(*o*-Carboxyphenyl)-2-chloro-5-[2-{bis(2-pyridylmethyl)amino-methyl}-*N*-methylaniline]-6-hydroxy-3-xanthanone (ZP4, 14). 2′-Chloro-5′-bromo-methylfluorescein di-*tert*-butyldimethylsilyl ether (**8**, 160 mg, 234 µmol) and pyridine (85 µL, 1.1 mmol) were combined in 7 mL of CH₃CN. AgNO₃ (60 mg, 349 µmol) was added to the stirring solution causing the reaction to change from a yellow solution to a clear solution with the formation of a white precipitate. After 15 min, 2-[bis(2-pyridylmethyl)aminomethyl]-aniline (**11**) in 20 mL of CH₃CN was added to the solution, and the reaction mixture was stirred for 12 h at room temperature. The crude reaction mixture was filtered through Celite and diluted with brine (~300 mL), EtOAc (200 mL) and CH₂Cl₂ (100 mL). The combined organics were washed with brine (35 100 mL), dried over Na₂SO₄, and the solvents were removed to give TBS-protected ZP4. The crude product was combined in 15 mL of THF with AcOH (32 µL, 538 µmol) and 1.0 M tetrabutylammonium fluoride (TBAF in THF, 485 µL, 485 µmol) and stirred for 36 h at room temperature. Upon addition of the TBAF, the solution immediately changed from orange to deep red. The reaction was diluted with 100 mL of H₂O, and the aqueous solution was washed with hexanes (2 × 100 mL) then saturated with NaCl. The product was extracted into EtOAc, and the combined organics were washed with H₂O (100 mL) and brine (3 × 100 mL), dried over Na₂SO₄ to give a red solid after filtration and solvent removal. Medium-pressure flash chromatography on RP18 silica (3:1 0.1 N HCl:CH₃CN) followed by removal of the CH₃CN afforded an acidic solution of ZP4. The acidic solution was loaded onto a second RP18 silica column packed with millipure H₂O, and the column was washed with millipure water until the elutant from the column reached neutral pH (6−7, pH paper). The product was washed off the column (4:1 CH₃CN/H₂O), and the solvents were removed to give an orange powder (48 mg, 30%). ¹H NMR (DMF-d₇, 500 MHz) δ 3.78 (1 H, d, $J = 22$ Hz), 3.88 (1 H, d, $J = 24.5$ Hz), 3.92 (2 H, d, $J = 25.5$ Hz), 4.00 (2 H, d, $J = 24$ Hz), 4.59 (2 H, s), 6.59 (1 H, t, $J = 12$ Hz), 6.68 (1 H, d, $J = 14.5$ Hz), 6.80 (1 H, s), 7.01 (1 H, d, $J = 13.5$ Hz), 7.03 (1 H, d, $J = 14.5$ Hz), 7.16−7.20 (2 H, m), 7.25−7.29 (3 H, m), 7.43−7.51 (3 H, m), 7.69 (2 H, t, $J = 12.5$ Hz), 7.81 (1 H, t, $J = 11.5$ Hz), 7.90 (1 H, t, $J = 10.5$ Hz), 8.07 (1 H, d, $J = 12.5$ Hz), 8.40 (2 H, d, $J = 7.0$ Hz). ¹³C NMR (DMF-d₇, 125 MHz) δ 58.57, 60.02, 105.39, 111.18, 111.74, 112.30, 113.76, 113.87, 117.03, 117.61, 123.84, 124.87, 125.40, 125.93, 128.01, 128.74, 129.33, 130.37, 131.45, 132.62, 136.75, 138.95, 148.96, 149.32, 151.91, 152.16, 153.45, 156.91, 160.04, 169.82. FTIR (KBr) 3372, 3062, 1792, 1606, 1450, 1284, 1252, 754. HRMS (ESI): Calcd for MH⁺ 683.2061; Found 683.2024.

[2-{Bis(2-pyridylmethyl)aminomethyl}-*N*-methylaniline]phenol (BPAMP, 15). 2-[Bis(2-pyridylmethyl)aminomethyl]-aniline (**11**, 2.15 g, 7.06 mmol) was dissolved in 50 mL of EtOAc and salicylaldehyde (0.72 mL, 6.76 mmol) was added dropwise via a syringe. The reaction mixture was stirred for 12 h under Ar, and the solvent was removed. The resulting yellow oil was dissolved in 50 mL of dichloroethane, combined with NaBH(OAc)₃ (1.58 g, 7.45 mmol), and stirred vigorously for 12 h at room temperature. The excess NaBH(OAc)₃ was quenched with saturated NaHCO₃, and the product was extracted into CH₂Cl₂

(3 × 50 mL). The combined organics were washed once with water (50 mL), dried over $MgSO_4$, filtered, and the solvent was removed to give a dark yellow oil. Flash chromatography on silica ($CHCl_3$/MeOH/ *i*-$PrNH_2$ 195:4:1) yielded the product as a yellow solid (1.98 g, 71.2%). TLC R_f = 0.26 ($CHCl_3$/MeOH/$^iPrNH_2$ 195:4:1). ¹H NMR ($CDCl_3$, 300 MHz) δ 3.48 (2 H, s), 3.56 (4 H, s), 4.27 (2 H, d, J = 7.0 Hz), 6.45– 6.55 (2 H, m), 6.69–6.73 (2 H, m), 6.84–6.93 (4 H, M), 7.00–7.04 (3 H, m), 7.09 (1 H, d, J = 12.5 Hz), 7.28 (2 H, td, J = 1.5, 2.5 Hz), 8.25 (2 H, dt, J = 1.0, 8.0 Hz).¹³C NMR ($CDCl_3$, 125 MHz) δ 46.46, 58.74, 60.52, 112.07, 116.91, 117.71, 119.74, 122.15, 123.40, 123.49, 125.38, 128.46, 128.71, 129.16, 130.82, 136.64, 147.69, 148.69, 156.55, 158.40. FTIR (thin film) 3294, 3042, 2818, 2717, 1592, 1455, 1237, 750. HRMS (ESI): Calcd for MH^+ 411.2179; Found 411.2160.

[Zn(BPAMP)(H₂O)](ClO₄) (16). A portion of BPAMP (**15**, 25 mg, 61 μmol) was combined with NaOH (0.81 mL, 0.075 M, 61 μmol) and zinc triflate (0.81 mL, 0.075 M, 61 μmol) in 3 mL of CH_3CN. Sodium percholrate (200 mg, 1.6 mmol) was dissolved in water (1 mL) and added to the CH_3CN solution, then the combined solutions were filtered through Celite. Crystallization at room temperature with concurrent evaporation of some solvent over 2 days yielded yellowish clear blocks suitable for X-ray crystallography. The crystalline material was filtered, powdered, and dried under vacuum at 50 °C to yield 14.2 mg of product in 39.4% yield. FTIR (KBr) 3490, 3270, 3062, 2860, 1607, 1478, 1446, 1274, 1099, 761, 622. Anal. Calcd for $ZnC_{26}H_{27}$- $Cl_1N_4O_6$: C, 52.72; H, 4.59; N, 9.46. Found: C, 52.47; H, 4.52; N, 9.28.

[Mn(BPAMP)(H₂O)](ClO₄) (17). BPAMP (**15**, 40 mg, 97 μmol) was combined with NaOH (1.3 mL, 0.075 M, 97 μmol) and manganese perchlorate (1.3 mL, 0.075 M, 97 μmol) in 3 mL of MeOH. The MeOH solution was layered with water (3 mL) containing sodium percholrate (300 mg, 2.4 mmol). Crystallization at room temperature with concur- rent evaporation of some solvent over 2 d yielded clear yellow blocks suitable for X-ray crystallography. The crystalline material was filtered, powdered and dried under vacuum at 50 °C to yield 36.2 mg of dried product in 64.1% yield. FTIR (KBr) 3469, 1605, 1477, 1444, 1270, 1109, 1094, 764, 622. Anal. Calcd for $MnC_{26}H_{27}Cl_1N_4O_6$: C, 53.66; H, 4.68; N, 9.63. Found: C, 53.71; H, 4.78; N, 9.75.

[Cu(BPAMP)](ClO₄) (18). This compound was prepared in a manner identical to that described above for **17** using copper perchlorate (1.3 mL, 0.075 M, 97 μmol) and crystallized as brown needles and green blocks. Only the green blocks were suitable for X-ray crystal- lography. The crystalline material was filtered, powdered and dried under vacuum at 50 °C to yield 36.2 mg of dried product in 71.3% yield. FTIR (KBr) 3431, 3239, 3072, 2926, 1607, 1478, 1446, 1276, 1092, 758, 621. Anal. Calcd for $CuC_{26}H_{25}Cl_1N_4O_5$: C, 54.55; H, 4.40; N, 9.79. Found: C, 54.31; H, 4.46; N, 9.89.

Collection and Reduction of X-ray Data. Crystals were covered with Paratone-N oil and suitable specimens were mounted on the tips of glass fibers at room temperature and transferred to a Bruker (formerly Siemens) APEX X-ray diffraction system with a graphite-monochro- matized Mo Kα radiation (λ = 0.710 73 Å) controlled by a Pentium- based PC running the SMART software package.[44] Data were collected at 173 K in a stream of cold N_2 maintained with a KRYO–FLEX nitrogen cryostat. Procedures for data collection and reduction have been reported previously.[45] The structures were solved by direct methods and refined by full matrix least-squares and difference Fourier techniques with SHELXTL.[46] Empirical absorption corrections were applied with the SADABS program,[47] and structures were checked for higher symmetry by PLATON.[48] Space groups were determined by examining systematic absences and confirmed by the successful solution

and refinement of the structures. All non-hydrogen atoms were refined anisotropically. Hydrogen atoms were assigned idealized locations and given isotropic thermal parameters 1.2 times the thermal parameter of the carbon atoms to which they were attached. In the structures of **16** and **18**, the perchlorate anion is disordered, and a water molecule in both **16** and **17** is partially occupied; all were modeled and refined accordingly. Relevant crystallographic information is contained in the Supporting Information, and the 50% thermal ellipsoid plots are shown in Figure 2.

General Spectroscopic Methods. Ultrol grade PIPES (piperazine- *N,N′*-bis(2-ethanesulfonic acid)) from Calbiochem and KCl (99.997%) was purchased and used as received. All solutions were passed through 0.2-μM cellulose filters before measurements. Except for the fluores- cence titration experiment, Zn solutions were prepared by the addition of appropriate amounts of 1.0 M, 100 mM, 10 mM or 1 mM Zn^{2+} stocks that were checked by atomic absorption spectroscopy for concentration accuracy, or by titration with terpyridine and measurement of the absorption spectra. The titration was performed by treating a 100 mM solution of 2,2′:6′,2″-terpyridine in buffered solution (50 mM PIPES, 100 mM KCl, pH 7) with aliquots of 10 mM (nominal) $ZnCl_2$ and determining the equivalence point by monitoring the absorbance of the resulting complex at 321 nm (ϵ = 35.9 × 10^3 M^{-1} cm^{-1}). The Zn^{2+} stocks were prepared from 99.999% pure $ZnCl_2$. The purity of the ZP probes was verified by HPLC on an analytical RP18 column using a 0.1% aqueous TFA:CH_3CN solvent gradient. The purity of the ZP probes was verified by HPLC. ZP was introduced to aqueous solutions by addition of a stock solution in DMSO (0.67 mM). Graphs were manipulated and equations calculated by using Kaleidagraph 3.0. The pH values of solutions were recorded with an Orion glass electrode that was calibrated prior to each use. The experiments for measuring the pH-dependent fluorescence, quantum yield, K_d, metal ion selectivity were performed as previously described.[38–40,49]

Titration of ZP1, ZP4, and BPAMP with Metal Ions. Solutions (50 mM PIPES, 100 mM KCl, pH 7) containing either 10 μM ZP1, 10 μM ZP4 or 100 μM BPAMP were titrated with 10 mM stock solutions of the divalent metal ion under consideration ($CuCl_2$, $MnCl_2$ or $ZnCl_2$). The absorption spectrum for each trial was measured before and following the addition of each aliquot of stock solution. Subtraction of the initial spectrum from subsequent ones generated absorption difference plots. The absorption changes were plotted as a function of $[M^{2+}]$.

UV–Visible Spectroscopy. Absorption spectra were recorded on a Hewlett-Packard 8453A diode array spectrophotometer under the control of a Pentium II-based PC running the Windows NT ChemStation software package, or a Cary 1E scanning spectrophotometer under the control of a Pentium PC running the manufacturer supplied software package. Spectra were routinely acquired at 25 °C, maintained by a circulating water bath in 1-cm path length quartz cuvettes with a volume of 1.0 or 3.5 mL.

Fluorescence Spectroscopy. Fluorescence spectra were recorded on a Hitachi F-3010 spectrofluorimeter under the control of a Pentium- based PC running the SpectraCalc software package. Excitation was provided by a 150 W Xe lamp (Ushio Inc.) operating at a current of 5 A. All spectra were normalized for excitation intensity via a rhodamine quantum counter, and emission spectra were normalized by the manufacturer-supplied correction curves. Spectra were routinely acquired at 25 °C, maintained by a circulating water bath in 1 × 1 cm quartz cuvettes using 3 nM slit widths and a 240 nm/min scan speed. All spectra were corrected for emission intensity by using the manufacturer-supplied photomultiplier curves.

Tissue Preparation and Staining Procedures. Tissue from normal rats suffering prior seizures was used. Methods of administering

(44) *SMART*; 5.626 ed.; Bruker AXS, Inc.: Madison, WI, 2001.
(45) Feig, A. L.; Bautista, M. T.; Lippard, S. J. *Inorg. Chem.* **1996**, *25*, 6892– 6898.
(46) Sheldrick, G. M. *SHELXL97–2: Program for the Refinement of Crystal Structures*; University of Gottingen: Germany, 1997.
(47) Sheldrick, G. M. *SADABS: Area-Detector Absorption Correction*; Uni- versity of Gottingen: Germany, 1996.
(48) Spek, A. L. *PLATON, A Multipurpose Crystallographic Tool*; Utrecht University: Utrecht, The Netherlands, 1998.
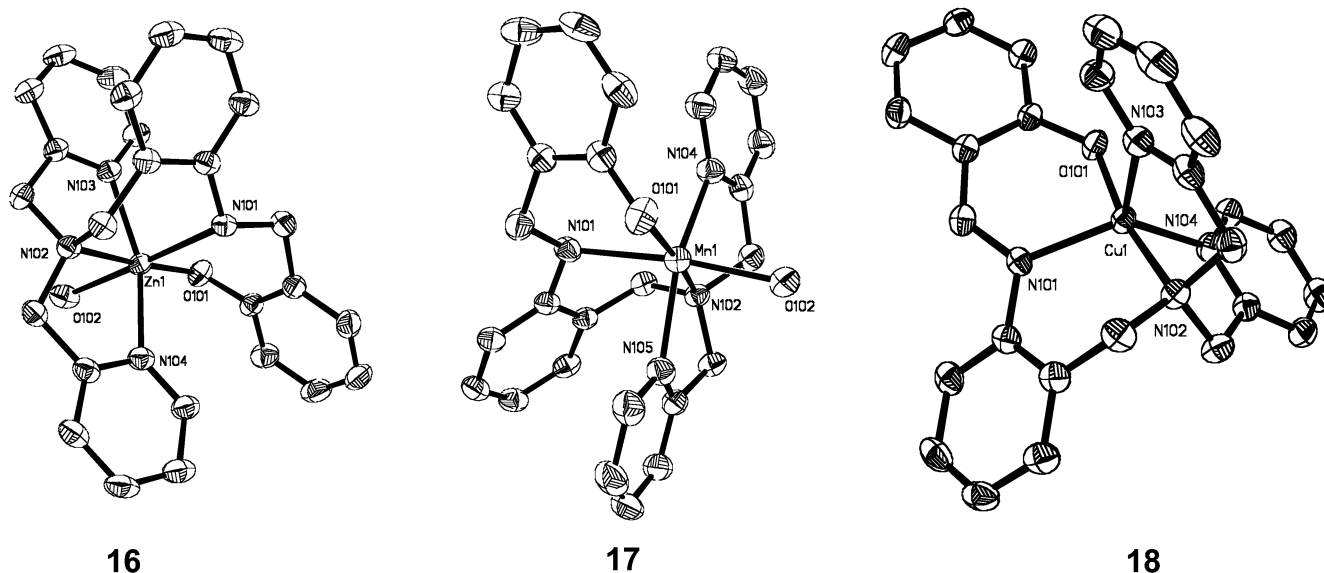(49) Walkup, G. K.; Burdette, S. C.; Lippard, S. J.; Tsien, R. Y. *J. Am. Chem Soc.* **2000**, *122*, S1–S7.

16   **17**   **18**

Figure 2. ORTEP diagrams of [Zn(BPAMP)(H₂O)](ClO₄)·0.5(H₂O) (**16**·0.5H₂O), [Mn(BPAMP)(H₂O)](ClO₄)·(CH₃OH)·0.5(H₂O) (**17**·CH₃OH·(0.5)H₂O) and [Cu(BPAMP)(H₂O)](ClO₄) (**18**) showing 50% thermal elipsoids and selected atom labels. Solvent molecules, hydrogen atoms and perchlorates are omitted for clarity. Selected bond lengths (Å) and angles (deg) for **16**: Zn(1)−O(101) = 1.9795(15), Zn(1)−O(102) = 2.1134(17), Zn(1)−N(101) = 2.3048(17), N(101)−Zn(1)−O(102) = 175.97(6); **17**: Mn(1)−O(101) = 2.0546(19), Mn(1)−O(102) = 2.182(2), Mn(1)−N(101) = 2.360(2), N(101)−Mn(1)−O(102) = 172.86(7); **18**: Cu(1)−O(101) = 1.894(2), Cu(1)−N(101) = 2.004(3), O(101)−Cu(1)−N(101) = 94.65(11), N(101)−Cu(1)−N(102) = 95.92(12).

Scheme 1
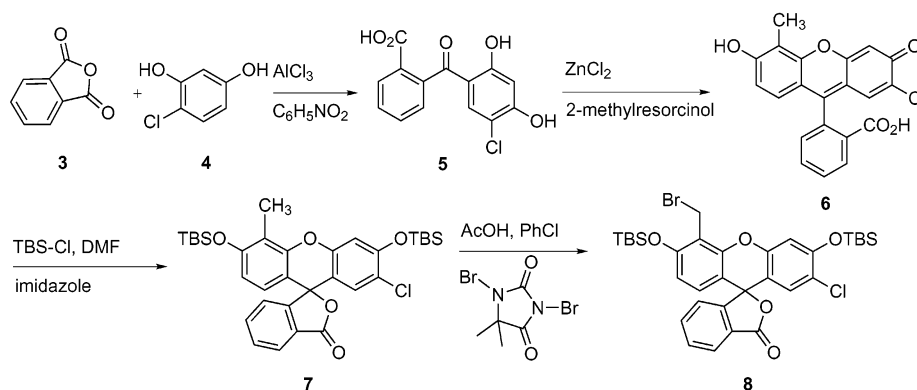
pilocarpine by intraperitoneal injection were followed,[50] and the rats were allowed to survive overnight after drug administration. After seizure or control (no) treatment, rats were killed by an overdose of anesthesia, decapitated, and the brains were removed rapidly and frozen by burying on dry ice "snow" for 2−3 min. Frozen brains were then mounted on the chuck of a closed-cabinet cryostat (Harris/Jung Reichert), and cut (at −13 °C) at anywhere from 6 to 30 μm thickness. Immediately after thawing onto clean glass slides, the sections were allowed to dry at room temperature for 0.5 to 3 h, then stained and photographed. Through all steps, care was taken to keep sections covered in dust-free containers.

Staining was done by applying 60 μL of staining fluid to sections lying flat in a plastic box. After 1 min, the excess reagent was washed off by gentle agitation in a 0.8% saline solution. Slides were viewed and photographed while still damp without coverslips, immediately after rinsing. To improve contrast, selected sections were also cleared by immersion in increasing concentrations of glycerol (in water), specifically 30, 60, 90, and 100%. These were then viewed under glycerine immersion (Zeiss 25×, variable aperture) with 1.25 or 2.0-post magnification.

Microscopy Methods. Images were made on a Zeiss Universal with SPOT II cooled CCD camera, using Olympus Plan-apo 10× (0.87) or

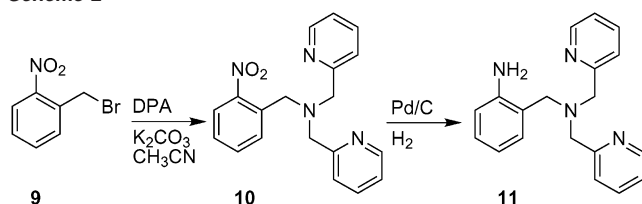(50) Suh, S. W.; Thompson, R. B.; Frederickson, C. J. *Neuroreport* **2001**, *12*, 1523−1525.

Zeiss 25× (glycerine or water immersion, 1.3). Illumination was via 200 W HBO high-pressure mercury illumination, using either a 360 or 480 nm excitation band-pass filter, 500 nm dichroic splitter and either a long-pass or a 550 band-pass emission filter. Additional images were made on a Nikon Diaphot with Odyssey confocal, illuminating with 488 nm Argon laser and viewing through a 500 nm long-pass filter. In this case, sections were mounted directly on coverslips and viewed (from below) through the coverslip with oil immersion, using Nikon 40 and 100× objectives.

Results

ZP4 Synthesis. Scheme 1 outlines the synthesis of the fluorescein scaffold from commercially available starting materials. Multigram quantities of 2′-carboxy-5-chloro-2,4-dihydroxybenzophenone (**5**) can be prepared in 49% yield by reacting 1 equiv of phthalic anhydride (**3**) and 4-chlororesorcinol (**4**) using AlCl₃ as a catalyst. Subsequent fusion of **5** with 2-methylresorcinol using ZnCl₂ as the catalyst yields a mixture of the desired 2′-chloro-5′-methylfluorescein (**6**), 2′,7′-dichlorofluorescein and 4′,5′-dimethylfluorescein. The crude reaction mixture consists of a 4:1 ratio of the desired asymmetric product and the symmetric byproducts. The dichlorofluorescein is removed during workup, leaving a mixture containing ~90%

Scheme 2

6. Silylation of the phenols on both fluorescein components with *tert*-butyldimethyl silyl chloride (TBS−Cl) under standard conditions provides 2′-chloro-5′-methylfluorescein di-*tert*-butyl-dimethylsilyl ether (**7**) in 37% yield based on NMR integration. Bromination of the mixure of silylated products under mild conditions and removal of the remaining symmetric product by flash chromatography gives 2′-chloro-5′-bromomethylfluorescein di-*tert*-butyldimethylsilyl ether (**8**) in 73% yield (13% overall). Scheme 2 outlines the synthesis of the ligand fragment from the commercially available 2-nitrobenzyl bromide (**9**) using conventional methods. The overall yield for **11** is only 3% because of the low-yielding reduction of the nitro group.

The combination of fluorescein scaffold **8** and the ligand fragment **11** in the presence of AgNO₃ provides the silyl-protected final product (Scheme 3). Upon removal of the silyl groups with fluoride ion, pure ZP4 (**14**) is obtained after chromatography on reverse phase silica. Analysis of the crude product suggests a >50% conversion to ZP4 that is >80% pure. The most significant loss of product occurs during chromatography. The overall yield of ZP4 is 4% from 4-chlororesorcinol.

Fluorescence Properties of ZP4. Figure 3 depicts the pH dependent fluorescence changes measured for ZP4. The plot of the integrated emission intensity reveals three fluorescence-related pK_a values: a slight emission enhancement with a pK_a of 10.0, a larger increase with a pK_a of 7.2, and fluorescence quenching with a pK_a of 4.0.

In buffered solution (50 mM PIPES, 100 mM KCl, pH 7) using EDTA to scavenge adventitious metal ions, ZP4 has a quantum yield of 0.06 and an emission maximum at 521 nm.
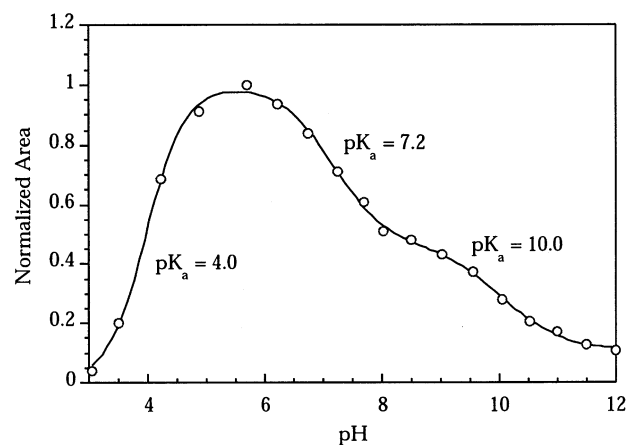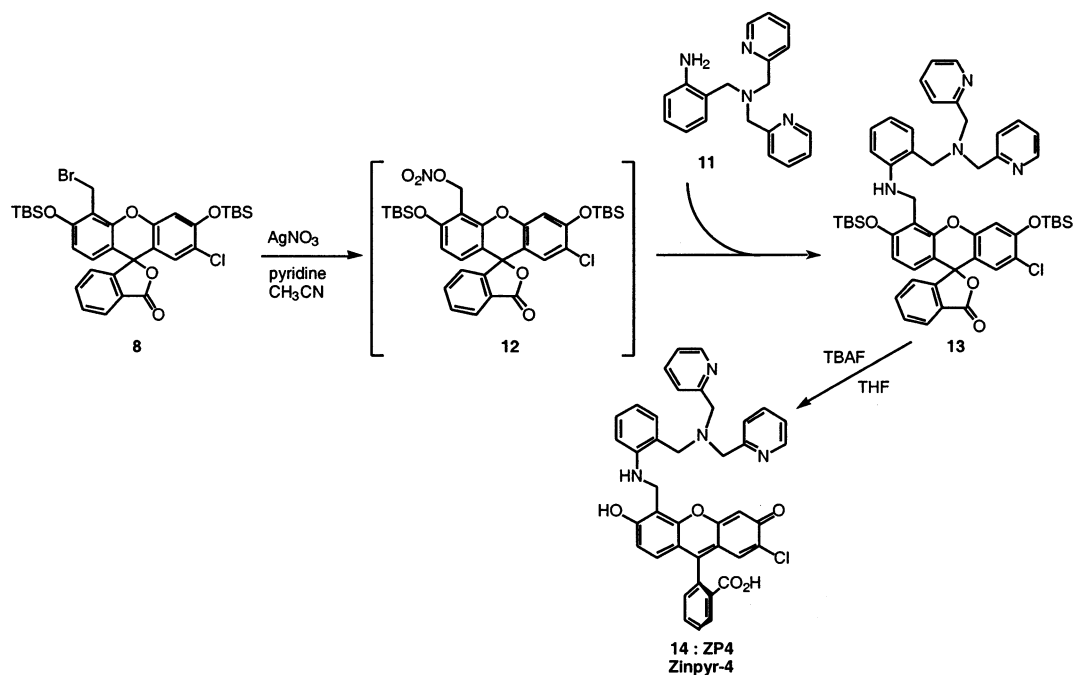

Figure 3. Plot of the normalized integrated emission intensity versus pH for ZP4. The pK_a at 10.0 correspond to the aliphatic nitrogen and the one at 7.2 to the aniline nitrogen. At low pH fluorescein adopts a nonfluorescent isomer corresponding to the decrease in emission intensity. The quantum yield of the sensor at pH 7 is 0.06.

Upon the addition of 25 μM Zn²⁺, the quantum yield increases to 0.34 and the emission maximum shifts to 515 nm. The addition of Zn²⁺ is also accompanied by a shift in the excitation maximum from 506 nm ($\epsilon = 61.0 \times 10^3$) to 495 nm ($\epsilon = 66.7 \times 10^3$). The brightness ($\epsilon \times \Phi$) of the Zn²⁺-bound sensor is (22.7×10^3).

The fluorescence response of ZP4 is Zn²⁺- and Cd²⁺-selective. Figure 4 shows the fluorescence response of ZP4 in the presence of various divalent metal ions. Even high concentrations (2 mM) of Ca²⁺ and Mg²⁺ produce no appreciable change in the fluorescence emission. Fluorescence enhancement of ZP4 by Zn²⁺ occurs in the presence of these two metal alkali earth metal ions. Other first row transition metals including Cu²⁺, Ni²⁺, Co²⁺, Fe²⁺, and Mn²⁺ produce no discernible change in the emission intensity, but only the sample containing Mn²⁺ affords a fluorescence response upon the subsequent addition of Zn²⁺.
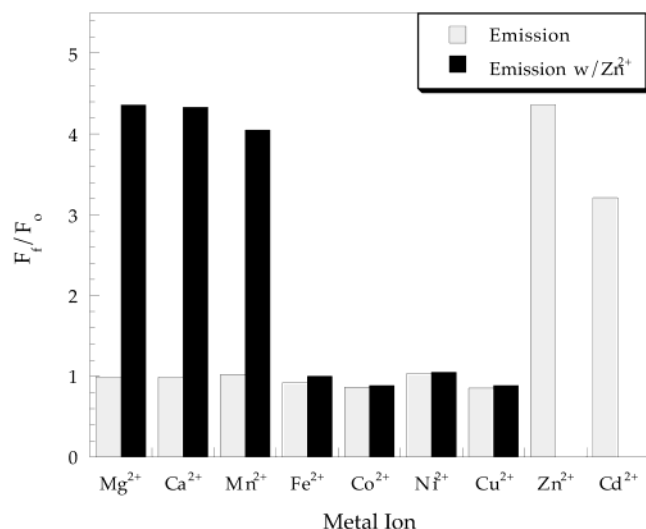
Scheme 3

Figure 4. Fluorescence response of ZP4 to various metal ions. Bars represent the final integrated fluorescence response (F_f) over the initial integrated emission (F_i). Initial spectra were acquired in 100 mM KCl, 50 mM PIPES, 10 μM EDTA pH 7.00 at 25 °C. Excitation was provided at 500 nm, and the emission was integrated between 503 and 635 nm. Aliquots of concentrated stock solutions (10 mM) of each metal ion were added to the solution to provide 50 μM total metal ion. Zn^{2+} solution was added to the solution containing the metal ion similarly.

The binding affinity of ZP4 was characterized by using the dual-metal single-ligand buffer system described previously.[38,40] Varying the total Zn^{2+} concentration between 0 and 1 mM while maintaining constant concentrations of Ca^{2+} (2 mM) and EDTA (1 mM) provides buffered free Zn^{2+} between 0.17 and 25 nM. The quantum yield of ZP4 increases 5.7-fold upon the addition of Zn^{2+}; similarly, the integrated emission intensity increases ~5-fold during the binding titration. Figure 5 shows a representative titration of ZP4 and the fitting of the integrated fluorescence emission. The titration was performed four times using different $Ca^{2+}/Zn^{2+}/EDTA$ buffers. Analysis of the response indicates that the [Zn(ZP4)] complex has an apparent K_d of 0.65 ± 0.10 nM.

Structural Features of ZP4. Attempts to crystallize the Zn^{2+} complex of ZP4 were unsuccessful, so a truncated version that includes the metal ion binding fragment, BPAMP, was prepared from **11** and salicylaldehyde (Scheme 4) in 71% yield. The Zn^{2+}, Mn^{2+} and Cu^{2+} complexes of the BPAMP ligand were crystallized from aqueous MeOH or CH_3CN in the presence of excess $NaClO_4$. All three complexes are monomers containing a single ligand and metal ion (Figure 2). The Mn and Zn compounds are isomorphous with the pentavalent ligand and a water molecule forming a distorted octahedral complex. The Cu complex lacks the water molecule, adopting distorted trigonal bipyramidal geometry.

Titrations of ZP4 and BPAMP in buffered solution with Zn^{2+} show 1:1 binding by optical spectroscopy. Titration of ZP1 exhibits 2:1 ZP1:Zn^{2+} binding accompanied by changes in the absorption spectrum similar to those observed for ZP4. The titration of ZP1 and ZP4 with Cu^{2+} and Mn^{2+} also reveals 2:1 and 1:1 binding, respectively.

Histological Staining Results. In contrast to 6-methoxy-(8-*p*-toluenesulfonamido)quinoline (TSQ), which stains all of the zinc-containing terminal fields in hippocampal slices (Figure 6b), slices treated with ZP4 only show intense staining of the
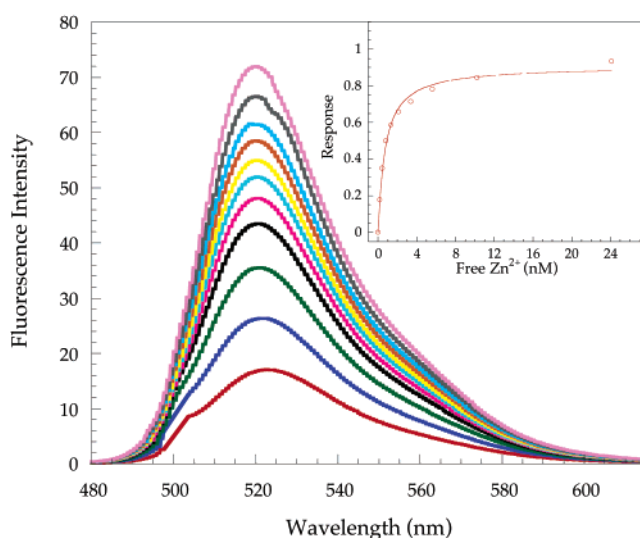

Figure 5. Fluorescence emission response of ZP4 to buffered Zn^{2+} solutions. Spectra were acquired in 100 mM KCl, 50 mM PIPES, pH 7.00 at 25 °C. Excitation was provided at 500 nm with 3 nm slit widths. Emission data were corrected for the response of the detector, using the manufacturer supplied curve, and the emission data points at 500 nm, which were perturbed by scatter, have been removed for clarity. The spectra shown are for free zinc buffered at 0, 0.172, 0.424, 0.787, 1.32, 2.11, 3.34, 5.60, 10.2, and 24.1, nM, respectively. For the final spectrum (containing 1 mM EDTA and 1 mM Zn^{2+}) additional $ZnCl_2$ was added to provide ~25 μM free Zn^{2+}. Inset: fluorescence response obtained by integrating the emission spectra between 503 and 635 nm, subtracting the baseline (0 Zn^{2+}) spectrum and normalizing to the full scale response (25 μM free Zn^{2+}).

Scheme 4
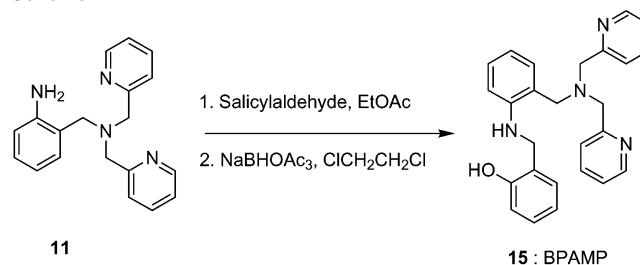
neurons injured by prior excitotoxic insult (seizures), with negligible labeling of zinc-containing vesicles (Figure 6a). Control slices show no detectable free zinc except in presynaptic vesicles that are only stained by TSQ.

Discussion

Synthesis. The synthetic approaches to both ZP1 and ZP2 result in a symmetric ligand substitution pattern at the 4′ and 5′ positions of the xanthenone ring (Figure 1).[38] Computer modeling suggested that binding a single Zn^{2+} ion between ligands emanating from these two positions would be geometrically and entropically disfavored. One possible strategy for making a sensor with a single Zn^{2+}-binding site is to incorporate the metal-binding moiety on the bottom (phthalate) ring. Synthesis of bottom ring modified fluorescein derivatives from resorcinol and phthalic anhydride derivatives inevitably requires a difficult separation of structural isomers, however. Fluorescein amine is a commonly employed, commercially available bottom ring derivative; however, it is not an attractive starting material because of its high cost and the relative inertness of the amino group to chemical transformation. In addition to expense and reactivity, bottom ring synthetic strategies often require low
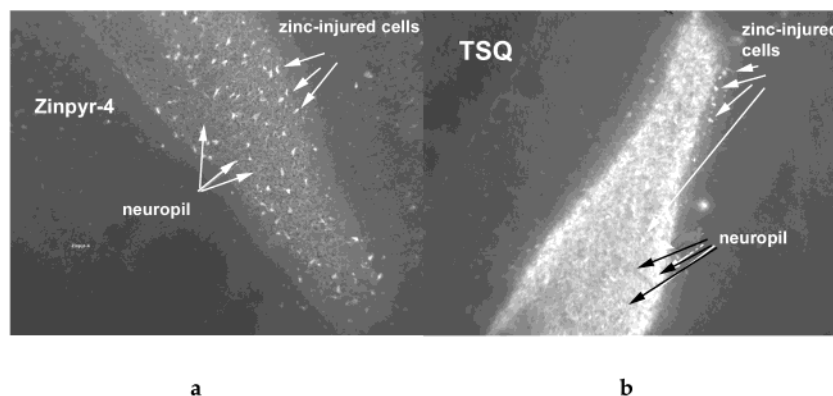
Figure 6. Hilus of dentate gyrus stained with (a) ZP4 and (b) TSQ. The brain tissue is taken from a rat following seizure activity. The zinc-positive neurons are more distinct when labeled with ZP4 because the neuropil are not stained. The background from Zn^{2+}-containing vesicles that are stained by TSQ makes identification of damaged cells more difficult.

yielding, multistep processes that subject the fluorescein to rigorous reaction conditions and difficult purification after each manipulation.[51] Alternatively, we envisioned adapting the method used to prepare ZP2 to access unsymmetrical fluorescein derivatives with a single zinc-binding moiety on the xanthenone ring.

An unsymmetrical fluorescein-based Ca^{2+} sensor was the inspiration for our synthetic strategy.[52] In the conventional synthesis of fluoresceins, 2 equiv of a resorcinol are allowed to react with phthalic anhydride under rigorous conditions to give the product. Two molecules of resorcinol condense to form the xanthenone skeleton. To obtain a fluorescein with a single metal-binding arm, a strategy that employs two different resorcinols is required. Dihydroxybenzophenone derivatives such as 2′-carboxy-5-chloro-2,4-dihydroxybenzophenone (**5**) are intermediates in the formation of fluorescein molecules. When prepared independently from 4-chlororesorcinol (**4**) and phthalic anhydride (**3**), **5** reacts with 2-methyl resorcinol to give an asymmetric fluorescein (Scheme 1). Analysis of the reaction product reveals minor amounts of 2′,7′-dichlorofluorescein and 4′,5′-dimethylfluorescein. The presence of these symmetric fluoresceins indicates that the formation of the benzophenone is to some extent reversible. A variety of methods and catalysts were screened in an attempt to eliminate the formation of these symmetric products, but the highest conversion to the desired monofunctional fluorescein was 80% under $ZnCl_2$ fusion conditions.[53]

Separation of the 2′-chloro-5′-methylfluorescein (**6**) from the symmetric products proved to be both difficult and unnecessary. Installation of *tert*-butyldimethyl silyl (TBS) ethers on the phenols under standard conditions provides a convenient method to purify and manipulate the desired product. Unprotected fluoresceins are notoriously difficult to handle because of their limited solubility in conventional organic solvents and their propensity to adopt different isomeric forms. Silyl ethers were selected as the protecting groups for their stability to nucleophiles by comparison to esters that were utilized previously.[38] The similar polarity of silylated 4′,5′-dimethylfluorescein and 2′-chloro-5′-methylfluorescein di-*tert*-butyldimethylsilyl ether (**7**) prohibits separation, but following bromination the undesired

product could be removed by chromatography. Although the overall yield of 2′-chloro-5′-bromomethyl-fluorescein di-*tert*-butyldimethylsilyl ether (**8**) is moderately low, multigram quantities of this key fluorescein starting material can be obtained in several days.

A pre-assembled fluorescein starting material is an advantage for the convergent synthesis of target molecules. The primary significance of the synthesis outlined in Scheme 3 is the ability to modify the Zn^{2+}-binding ligand easily and logically to prepare future sensor candidates for screening. In addition to 2-nitrobenzyl bromide (**9**), a number of commercially available starting materials could serve as useful building blocks for the Zn^{2+}-binding fragment. Systematic variation of the ligand building block as well as the metal-binding fragment will permit correlation of structural features with fluorescence properties and the binding affinity of the probes. Another significant improvement in this synthetic method is the ability to access sensor molecules from the bromomethyl fluorescein derivative. Formation of a nitro-oxy compound in situ by combining **8** with $AgNO_3$ activates the benzylic position toward nucleophilic substitution. Displacement of the bromide facilitated by $AgNO_3$ activation avoids the low yielding oxidation chemistry required to prepare the dialdehyde precursor of ZP2.[38]

Fluorescence Properties of ZP4. Under simulated physiological conditions ZP1 and ZP2 exhibit relatively intense fluorescence in the absence of Zn^{2+} ($\Phi = \sim0.3$). This background emission decreases the sensitivity of these probes and interferes with the measurement of Zn^{2+} concentration gradients. The pK_a values of the amine responsible for the fluorescence change of ZP1 and ZP2 are 8.4 and 9.4, respectively. When the amines are completely deprotonated at high pH, both probes emit a dim fluorescent signal, and exhibit a dramatic fluorescence enhancement upon the addition of Zn^{2+}.[38] Because protonation diminishes the magnitude of the fluorescence change, adjusting the pK_a of the nitrogen responsible for the PET quenching attenuates the fluorescence properties. Aromatic nitrogen atoms typically have lower pK_a values ($pK_a = 4-6$) than their aliphatic counterparts. In addition to having a low affinity for protons, aniline nitrogen atoms seldom form strong bonding interactions with metal ions. To avoid proton interference while retaining an appreciable affinity for Zn^{2+}, ZP4 integrates an aniline nitrogen into a chelating ligand containing a di(2-picolyl)amine (DPA) moiety. Maintaining the delicate balance between Zn^{2+}-binding affinity and proton

(51) Hirano, T.; Kikuchi, K.; Urano, Y.; Higuchi, T.; Nagano, T. *J. Am. Chem. Soc.* **2000**, *122*, 12399−12400.
(52) Smith, G. A.; Metcalfe, J. C.; Clarke, S. D. *J. Chem. Soc., Perkin Trans. 2* **1993**, 1195−1204.
(53) Hilderbrand, S. H.; Lippard, S. J. **2000**, unpublished results.

Scheme 5
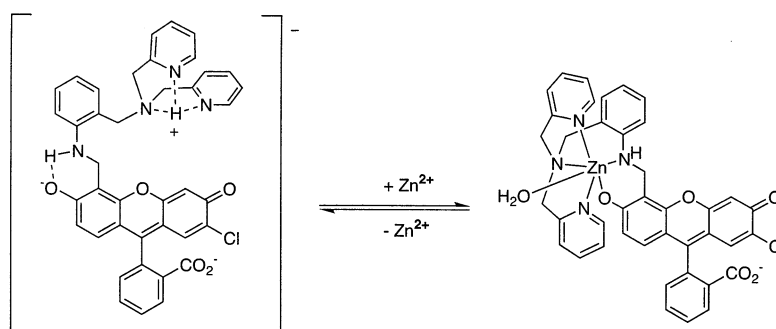
insensitivity represents the most significant challenge in designing PET-based Zn^{2+} sensors.

In the pH dependent fluorescence changes measured for ZP4, the pK_a at 10.0 corresponds to the protonation of the tertiary amine. Although the aniline nitrogen would be predicted to dominate PET, the aliphatic amine contributes to the quenching at basic pH. The high pK_a value of 10.0, compared to the value of ~9 for the previous ZP sensors, indicates that the environment of the aliphatic amine in ZP4 promotes binding of a proton. The pK_a of 7.2 measured for the aniline nitrogen provides additional evidence that advantageous H-bonding by the chelating ligand facilitates protonation. The pK_a associated with fluorescence quenching at low pH is consistent with the formation of a nonfluorescent fluorescein isomer that was observed for ZP sensors previously.[38] Lowering of the aniline pK_a will be addressed in future sensor design. Incorporation of electron withdrawing groups on the aniline ring, particularly the para position, should dramatically influence the pK_a of the aromatic nitrogen. The new convergent synthesis should facilitate easy access to related compounds.

The lower quantum yield (0.06) of the unmetalated sensor at pH 7, a value ~5-fold less than that observed for the previous generation ZP sensors, indicates that the aniline nitrogen more efficiently quenches fluorescence. The relatively low background emission from the free probe makes ZP4 a significant improvement over the first ZP sensors. Correlation of the Zn^{2+}-induced fluorescence enhancement with the pK_a measurements provides evidence that the aniline nitrogen also coordinates to the metal ion. Although the brightness of the Zn^{2+}-complexed sensor is sufficient for imaging applications, the quantum yield of the complex is less than half the value measured for ZP1 and ZP2. Possible explanations for the lower quantum yield of the Zn^{2+}-complex of ZP4 include the existence of a second unidentified quenching mechanism, or inefficient disruption of PET from the aniline nitrogen by Zn^{2+}-binding. Future investigation of structurally related ZP derivatives may help to understand the basis for this fluorescence behavior.

Structural Aspects of ZP4 and Behavior Toward Transition Metal Ions. The sub-nM Zn^{2+}-binding affinity of ZP4 is nearly identical to that of ZP1 and ZP2. In addition to Zn^{2+}-binding affinity, the hypsochromic shift in the absorption wavelength of ZP4 upon metal ion binding suggests that the phenolic oxygen coordinates to the Zn^{2+} ion in solution in the same manner as the previous two ZP sensors.[38] The similarity of the binding strength, the comparable absorbance and emission properties, and the use of an identical metal-binding ligand fragment indicate that the coordination of Zn^{2+} is probably similar for all three ZP complexes. The Zn^{2+}-induced shift in the absorbance spectrum is characteristic of binding by the phenolic oxygen. DPA has a high affinity for Zn^{2+} ($K_d = 70$ nM),[54] and the sub-nM K_d requires a contribution from this ligand fragment. The increase in quantum yield indicated coordination of the aniline nitrogen that is primarily responsible for PET quenching at physiological pH. Scheme 5 shows our interpretation of the solution chemistry of ZP4. In the absence of Zn^{2+}, the aliphatic amine is protonated, giving the sensor an overall -1 charge. Upon binding the chelating moiety wraps around the Zn^{2+} ion, with the final coordination site being occupied by a water molecule.

One of the most interesting aspects of ZP4 is the difference in the fluorescence behavior toward transition metal ions compared to properties of ZP1 and ZP2. This behavior indicates some difference in either the metal ion coordination or the electronic structure of the two generations of ZP metal complexes. Transition metal ions commonly quench the fluorescence of sensors.[42] Unlike the fluorescence of ZP1 and ZP2, which is quenched significantly by open shell metal ions, the emission of ZP4 is unchanged upon binding Mn^{2+}, Fe^{2+}, Co^{2+}, Ni^{2+}, and Cu^{2+}. Because subsequent addition of Zn^{2+} can only displace the weakly binding Mn^{2+} ion, it appears that the other transition metal ions bind tightly to the receptor of all three sensors and compete for the binding of Zn^{2+}. Examination of the optical spectra from the titration of ZP1 and ZP4 with Zn^{2+}, Cu^{2+}, and Mn^{2+} supports this conclusion, because the only apparent difference in the behavior of these two sensors is the stoichiometry of metal ion binding.

The crystal structure of the zinc complex of ZP1 contains two 5-coordinate Zn^{2+} ions each coordinated by the three nitrogen atoms of a DPA ligand, a phenolic oxygen and a water molecule.[38] The zinc coordination is identical to that of zinc[55] and other transition metal complexes[56,57] with truncated versions of this N_3O ligand. Since attempts to crystallize the Zn^{2+} complex of ZP4 were unsuccessful, BPAMP was used for structural studies. The BPAMP ligand shows Zn^{2+}-binding behavior similar to ZP4 in buffered solution. The crystal structures of the Zn^{2+}, Mn^{2+}, and Cu^{2+} complexes (Figure 2) display coordination consistent with the spectroscopic measurements of ZP4, with all 5 donors from the chelating ligand bound to the metal ions. The only difference between the 3 structures is that the Cu^{2+} complex is distorted trigonal bipyramidal rather

(54) Anderegg, G.; Hubmann, E.; Podder, N. G.; Wenk, F. *Helv. Chim. Acta* **1977**, *60*, 123−140.
(55) Trosch, A.; Vahrenkamp, H. *Eur. J. Inorg. Chem.* **1998**, 827−832.
(56) Uma, R.; Viswanathan, R.; Palaniandavar M.; Lakshminarayanan, M. *J. Chem. Soc., Dalton Trans.* **1994**, 1219−1226.
(57) Viswanathan, R.; Palaniandavar, M.; Balasubramanian, T.; Muthiah, T. P. *Inorg. Chem.* **1998**, *37*, 2943−2951.

than distorted octahedral because it lacks the coordinated water molecule found in the Zn^{2+} and Mn^{2+} structures. From the structural and spectroscopic experiments performed thus far, it remains unclear why the fluorescence response of ZP4 to transition metals is different from that of the first generation of ZP sensors. Investigation of the electronic structure of ZP4 complexes by DFT as well as experiments on the fluorescence properties is planned to investigate this behavior further.

These metal-binding properties have important implications in biological studies where other metal ions may interfere with Zn^{2+} measurements; however, there may be no such pools of available transition metals in healthy cells. The reducing environment within cells precludes the presence of Cu^{2+}, which is readily reduced to Cu^+ and disproportionates to Cu metal and Cu^{2+} in aqueous solution. Current evidence argues against the presence of free copper in cells and reveals that chaperone proteins transport Cu to its cellular targets.[58] Free Fe^{2+} readily oxidizes in aqueous solution to insoluble Fe^{3+},[59] drastically reducing the presence of free metal ion. Such Fe species would serve as a source of oxidative stress to cells,[60,61] so sequestration of Fe by macromolecules within cells seems extremely probable. Because most "free" transition metal ions seem to have a deleterious effect on living organisms,[62] numerous unidentified metalloregulatory proteins may exist, even for trace metals such as Co^{2+}. Despite the limited probability that other metal ions will interfere with biological assays, the ability to bind Zn^{2+} selectively in the presence of other transition metal ions remains an important goal in sensor design.

Imaging Damaged Neurons with ZP4. Because synaptic vesicles remain intact throughout slice preparation,[63] the inability of ZP4 to stain zinc-containing presynaptic terminals indicates that this probe cannot penetrate cellular membranes. In contrast to ZP4, membrane permeable probes such as TSQ and ZP1 stain these vesicles intensely. The impermeability of ZP4 may arise from either its charge at neutral pH, a dipole moment, or an inability to adopt a permeable lactone isomer.[64] Both the healthy

neurons and the cells damaged during seizures by the release of excitoxic Zn^{2+} are cut open by the microtome blade during tissue slicing, permitting ZP4 to enter the cells. Only the damaged neurons display intense fluorescence that indicates the presence of Zn^{2+} when stained. Because membrane permeable probes such as ZP1 and TSQ image both zinc-containing vesicles and damaged neurons, discrimination between the two is quite difficult. To date, ZP4 provides the most well resolved, detailed images of zinc-damaged neurons using fluorescence microscopy.[64]

Conclusions

We have designed, synthesized and characterized ZP4, a second-generation member of the ZP family of Zn^{2+}-selective sensors. ZP4 is prepared by a convergent synthesis where the fluorescein scaffold and the Zn^{2+}-binding fragment are prepared independently then linked to yield the final sensor. This new synthetic method, along with a high yielding synthesis of the key fluorescein intermediate, allows the efficient preparation of additional sensor candidates for screening. The key feature of ZP4 is the incorporation of an aniline nitrogen atom into the Zn^{2+}-binding ligand. The aniline nitrogen responsible for PET quenching of the unmetalated fluorophore has a lower pK_a than the aliphatic nitrogen of ZP1 and ZP2, making it is less sensitive to protonation under physiological conditions. Because the background fluorescence from free probe is diminished, ZP4 is more sensitive than previous ZP sensors.

Supporting Information Available: Figure S1 showing the fully labeled ORTEP diagrams of **16**−**18** and Tables S1−S12 showing pertinent crystallographic information for the 3 BPAMP complexes. This material is available free of charge via the Internet at http://pubs.acs.org.

JA0287377

(58) Rae, T. D.; Schmidt, P. J.; Pufahl, R. A.; Culotta, V. C.; O'Halloran, T. V. *Science* **1999**, *284*, 805−808.
(59) Crichton, R. R.; Pierre, J.-L. *Biometals* **2001**, *14*, 99−112.
(60) Joshi, J. G. *Ferritin: Intracellular Regulator of Metal Availability*; Connor, J. R., Ed.; Plenum Press: New York, 1997; pp 131−148.
(61) Glinka, Y.; Gassen, M.; Youdim, M. B. H. *Iron and Neurotransmitter Function in the Brain*; Connor, J. R., Ed.; Plenum Press: New York, 1997; pp 1−22.
(62) Connor, J. R. *Metals and Oxidative Damage in Neurological Disorders*; Plenum Press: New York, 1997.
(63) Mui, B. L.; Cullis, P. R.; Pritchard, P. H.; Madden, T. D. *J. Biol. Chem.* **1994**, *269*, 7364−7370.

(64) Frederickson, C. J.; Burdette, S. C.; Frederickson, C. J.; Sensi, S. L.; Weiss, J. H.; Balaji, R. V.; Bedell, E.; Prough, D. S.; Lippard, S. J., to be submitted for publication.